High Gain Electromagnetically Coupled Stacked Circular Disk Patch Antenna for Wideband Application

N. P. Yadav, W. Wu, and D. G. Fang
School of Optoelectronic, Nanjing University of Science and Technology, China

Abstract— Bandwidth enhancement behavior of an electromagnetically coupled stacked circular disk patch antenna is presented theoretically. The effects of feed point locations, radius of parasitic disk, and air gap-spacing are analyzed to achieve optimum conditions for wideband operation. The antenna shows a bandwidth as large as twelve times of that of a single circular patch antenna. The radiation patterns of the antenna are similar to those of the single disk antenna. The theoretical results are in reasonable agreement with the simulated ones from IE3D.

1. INTRODUCTION

A microstrip patch antenna has practical advantages such as low profile, light weight, low cost, and easy integration with printed circuits. One of the principal limitations of such antenna is its inherent narrow bandwidth which is of the order of few percent. It has been realized that bandwidth enhancement can be achieved by increasing effective volume of the patch antenna and introducing parasitic elements. The technique of stacking patches is one of the most popular ways to achieve broadband characteristic [1–3]. The present endeavor, therefore, is concerned with theoretical investigations in which bandwidth enhancement is achieved using two-layer electromagnetically coupled circular patch antenna. The theoretical investigations are carried out using cavity model and circuit theory concept. The theoretical results are compared with simulated results of the MoM based IE3D [4]. The details of investigations are given in the following sections.

2. THEORETICAL CONSIDERATIONS

The geometrical configuration of the two layered electromagnetically coupled stacked circular patch antenna is shown in Fig. 1. It consists of a driven circular patch of radius $a = 13.233$ mm and a parasitic circular patch of radius $b = 13.365$ mm. The driven patch is printed on a substrate material-I of relative permittivity $\varepsilon_{rd} = 2.45$ and thickness $h_d = 1.522$ mm. A coaxial probe of radius 0.564 mm excites the driven patch in TM_{11} mode of frequency 4.09 GHz. The probe feed is located at distance $a_f = 7.94$ mm from the center of the lower disk.

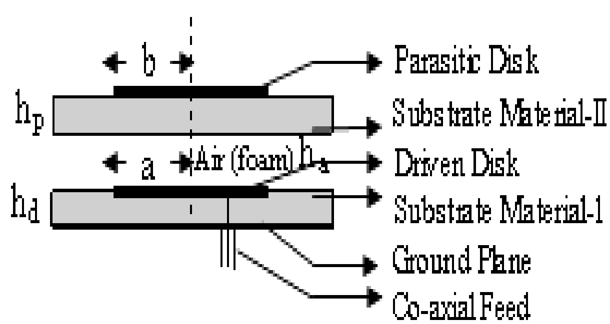

Figure 1: Geometrical configuration of the stacked antenna.

The parasitic patch is printed on a substrate material-II of thickness $h_p = 0.7609$ mm and dielectric constant $\varepsilon_{rp} = 2.45$. A foam material of relative permittivity $\varepsilon_{ra} = 1.22$ and thickness $h_a = 4.764$ mm is sandwiched between the two disks.

Under the assumptions of the cavity model, the stacked antenna can be considered to be consisting of two coupled cavity resonators, namely, lower cavity resonator and upper cavity resonator. The lower cavity resonator resembles a microstrip disk antenna covered with dielectric materials (foam and substrate material-II). Here, the effect of material of the upper patch may be neglected because fields are concentrated in the region between the lower patch and the ground plane. The upper cavity resonator consists of uncovered upper disk patch and the lower disk patch. The resonance frequencies of each resonator of the stacked disk antenna can be calculated using an approach similar to that of single microstrip disk antenna. Also, when a microstrip disk is covered by dielectric materials, the resonance behavior and the impedance characteristics are changed with relative permittivity, loss tangent, and thickness of the substrate material.

Being covered with super-substrate, the effective relative permittivity of substrate materials for lower disk resonator is given as [5]

$$\varepsilon_{ef} = \varepsilon_{ra} q_1 + \varepsilon_{req} \frac{(1-q_1)^2}{\varepsilon_{req}(1-q_1-q_2)+q_2} \tag{1}$$

where q_1 and q_2 are the filling factors defined for $a/h > 1$ [5]. Also, ε_{req} is the equivalent relative permittivity of the substrate materials above the lower disk and it is given as [6].

$$\varepsilon_{req} = \frac{\varepsilon_{ra}\varepsilon_{rp}(h_a+h_p)(1-\tan\delta_a\tan\delta_p)}{\varepsilon_{rd}h_a+\varepsilon_{ra}h_d} \tag{2}$$

The resonance frequency of TM_{11} mode for the lower disk resonator is given as

$$f_{rd} = \frac{\alpha_{11} c}{2\pi a_{eff}\sqrt{\varepsilon_{ef}}} \tag{3}$$

where $\alpha_{11} = k_{11}a$ is defined by $J'(k_{11}a) = 0$. Also, c is the velocity of light in free space and a_{eff} is the effective radius of lower disk, given as [7]

$$a_{eff} = a\left[1+\frac{2h_d}{\pi a\varepsilon_{ef}}\left(\ln\frac{\pi a}{2h_d}+1.7726\right)\right]^{1/2}; \quad \text{For } a/h \gg 1. \tag{4}$$

Based on the cavity model, the input impedance of a microstrip disk antenna may be computed by modeling the microstrip antenna as a parallel resonant LCR circuit. Therefore, the equivalent circuit of lower disk resonator may be represented as shown in Fig. 2(a). The circuit parameters of this resonator can be calculated as [8]

$$R_d = \frac{h_d^2 E_0^2 J_1^2(k_{11}a_f)}{2P_T} \tag{5}$$

$$C_d = \frac{\pi a^2 \varepsilon_0 \varepsilon_{ef}}{h}\left\{1+\frac{2h_d}{\pi a \varepsilon_{ef}}\left[\ln\frac{a}{2h_d}+1.41\varepsilon_{ef}+1.77+\frac{h_d}{a}(0.268\varepsilon_{ef}+1.65)\right]\right\} \tag{6}$$

$$L_d = \frac{1}{4\pi^2 f_{rd}^2 C_d} \tag{7}$$

Here, E_0 is the electric field intensity at the feed point and P_T is the total power lost that includes the power radiated and the power attenuated in the disk resonators owing to the finite conductivity of the disk conductor and imperfect dielectric substrate. Thus, from Fig. 2(a), the input impedance of the lower disk resonator can be derived as

$$Z_d = \frac{j\omega R_d L_d}{R_d - \omega^2 R_d L_d C_d + j\omega L_d} \tag{8}$$

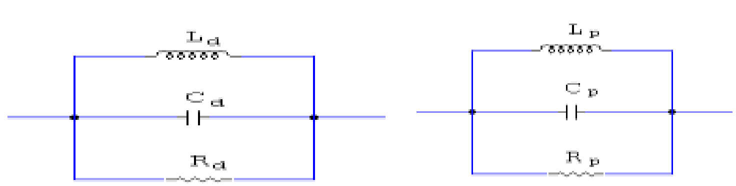

(a) (b)

Figure 2: Equivalent circuits of (a) driven disk, (b) parasitic disk.

As the upper parasitic patch is responsible for the upper disk resonator formed between the two disks, its resonance frequency can be given as

$$f_{rp} = \frac{\chi_{11} c}{2\pi b_{eff} \sqrt{\varepsilon_{req}}} \tag{9}$$

where $\chi_{11} = k_{11}b$ is defined by $J'(k_{11}b) = 0$ and b_{eff} is the effective radius of upper disk that can be computed using Equation (4) and replacing a, h_d, and ε_{ef} by b, $(h_p + h_a)$, and ε_{req} respectively. In addition, the equivalent circuit of the upper disk resonator is shown in Fig. 2(b), from which its impedance can be derived as

$$Z_p = \frac{j\omega R_p L_p}{R_p - \omega^2 R_p L_p C_p + j\omega L_p} \tag{10}$$

where, R_p, L_p, and C_p are the resonant resistance, inductance, and capacitance of the upper resonators. These parameters may be calculated using formulas (5)–(7) (Equations (5)–(7)) and replacing a, h_d, ε_{ef}, and f_{rd} by b, $(h_p + h_a)$, ε_{req}, and f_{rd} respectively.

Figures 3(a) & (b) show the current distributions on the lower driven disk patch and upper parasitic patch. Current flows on the lower patch due to coaxial feeding but the current on the upper parasitic patch is due to electromagnetic coupling between the two resonators.

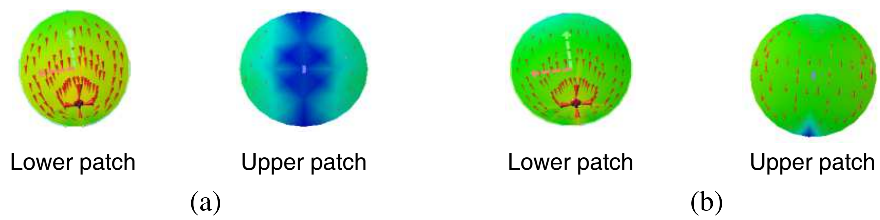

Figure 3: Current distributions on the patches at frequencies (a) 3.76 GHz and (b) 4.51 GHz.

The strength of current on the parasitic patch is dependent on the coupling coefficient. If L_m and C_m are the mutual inductance and mutual capacitance, the equivalent circuit showing electromagnetic coupling between two patches, may be represented as shown in Fig. 4(a). From the simplified equivalent circuit, shown in Fig. 4(b), the input impedance of the proposed stacked antenna can be derived as

$$Z_{in} = \frac{Z_d (Z_c + Z_p)}{Z_d + Z_c + Z_p} \tag{11}$$

Here, Z_c is the impedance due to inductive and capacitive coupling given as

$$Z_c = \frac{j\left(\omega^2 L_m C_m - 1\right)}{\omega C_m} \tag{12}$$

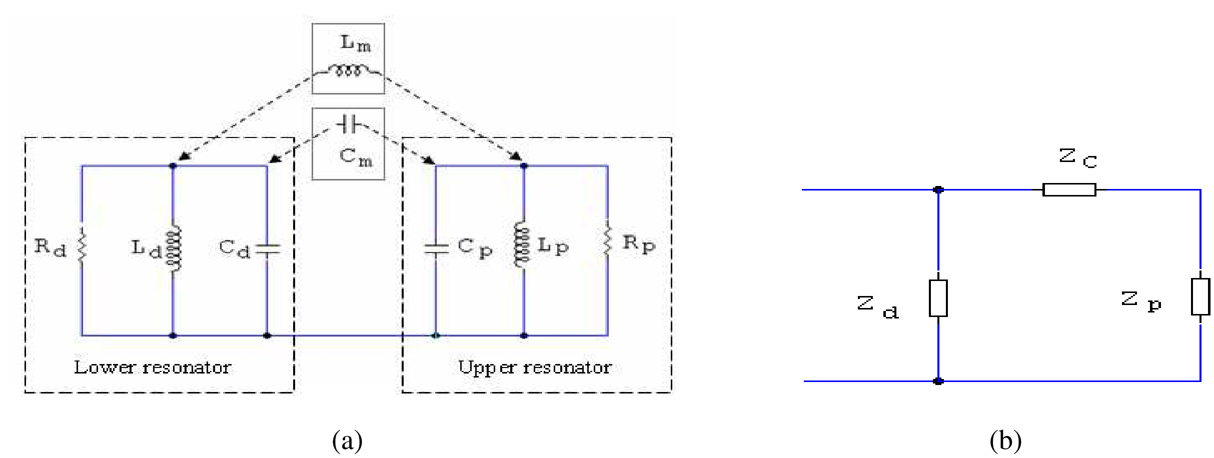

Figure 4: Equivalent circuits of proposed antenna (a) showing electromagnetic coupling and (b) after simplification.

The return loss value of the stacked antenna can calculated as

$$RL = -20 \log \frac{1+\Gamma}{1-\Gamma} \tag{13}$$

where $\Gamma = \frac{Z_{in}-Z_0}{Z_{in}+Z_0}$ and Z_0 is the characteristic impedance of the coaxial feed (50 ohms).

The bandwidth of the antenna can be evaluated as

$$BW = \frac{f_2 - f_1}{f_c} \times 100 \tag{14}$$

where f_1 and f_2 are the lower and upper frequency band-edges for return loss value ≤ -10 dB and f_c is the center frequency.

For dominant mode TM_{11}, the E-plane and H-plane radiation patterns of the antenna can be calculated by adding together the contributions of the fields due to lower and upper patches. Thus the radiation fields of the antenna can be given as [8]

$$E_\theta = -j^n \begin{bmatrix} \frac{V a_{\mathit{eff}} k_0}{2} \frac{e^{-jk_0 r}}{r} \cdot \cos\phi \cdot J_n' \left(k_0 a \sin\theta\right) + K_c \\ \frac{V b_{\mathit{eff}} k_0}{2} \frac{e^{-jk_0 r}}{r} \cdot \cos\phi \cdot J_n' \left(k_0 b \sin\theta\right) \end{bmatrix} \tag{15}$$

$$E_\phi = n j^n \begin{bmatrix} \frac{V a_{\mathit{eff}} k_0}{2} \frac{e^{-jk_0 r}}{r} \cdot \sin\phi \cos\theta \cdot \frac{J_n(k_0 a \sin\theta)}{k_0 a \sin\theta} + K_c \frac{V b_{\mathit{eff}} k_0}{2} \frac{e^{-jk_0 r}}{r} \\ \cdot \sin\phi \cos\theta \cdot \frac{J_n(k_0 b \sin\theta)}{k_0 b \sin\theta} \end{bmatrix} \tag{16}$$

where V is the radiating edge voltage, and r is the distance of an arbitrary far-field point, k_0 is the propagation constant in free space in TM_{11} mode, and K_c in coupling coefficient of the two resonators.

3. DISCUSSION OF RESULTS

The effect of feed location (a_f) on the antenna performance is shown in Fig. 5. It is observed that a_f has crucial effect in decreasing the mismatching of the antenna. It also affects the operational frequency band of the antenna and gives maximum frequency. Fig. 6 shows the effect of air gap-spacing (h_a) on the antenna performance. It is found that h_a plays a crucial role in controlling the resonance frequencies of the antenna and its matching as well. For low value of h_a, matching at lower resonance frequency improves, while at a higher resonance frequency the case is otherwise. Similarly, at higher value of h_a matching at higher resonance frequency improves and degrades at lower resonance frequency. The best matching at both resonance frequencies is achieved at $h_a = 4.76$ mm. The variation of return loss with frequency at different values of radius (b) of the

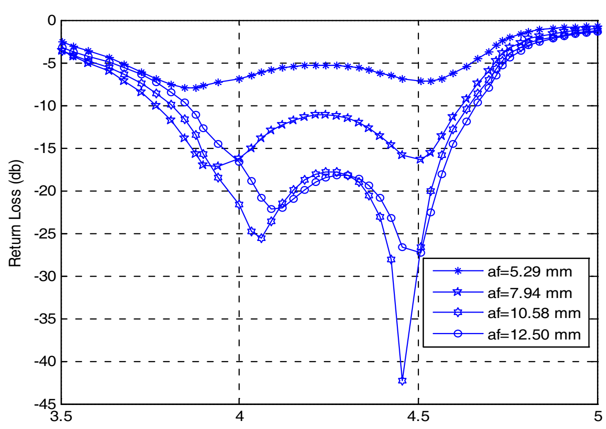

Figure 5: Return loss vs. frequency at different feed locations (a_f) for $a = 13.233$ mm, $b = 1.01a$, $\varepsilon_{rd} = \varepsilon_{rp} = 2.45$, $\varepsilon_{ra} = 1.22$, $h_d = 1.522$ mm, $h_a = 4.764$ mm, and $h_p = 0.7609$ mm, band for $a_f = 7.94$ mm.

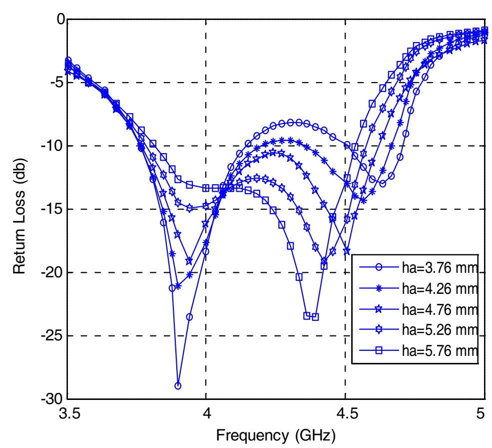

Figure 6: Return loss vs. frequency at different air gap-spacing (h_a) for $a = 13.233$ mm, $b = 1.01a$, $a_f = 7.94$ mm, $\varepsilon_{rd} = \varepsilon_{rp} = 2.45$, $\varepsilon_{ra} = 1.22$, $h_d = 1.522$ mm, and $h_p = 0.7609$ mm.

parasitic disk is shown in Fig. 7. It is observed that increase in b causes slight decrease in both the resonance frequencies but considerable decrease in frequency band. Also, it controls the matching effect of the antenna.

The optimum return loss curve at the optimum design parameters of the antenna is shown in Fig. 8, with a comparison between theoretical and simulated results. Theoretically, the antenna resonates at frequencies $f_1 = 3.9407$ GHz and $f_2 = 4.5085$ GHz. On the other hand, simulated results show resonances at $f_1 = 3.9696$ GHz and $f_2 = 4.4848$ GHz. From this figure it is noted that the antenna can operate with bandwidth of 19.79%, which is approximately twelve times the 1.66% bandwidth of single disk patch antenna.

The E- and H-plane radiation patterns of the optimized antenna at frequency 4.515 GHz are shown in Figs. 9 & 10. It is found that the 3-dB beam width of the antenna is 87.4° and 73° for E- and H-plane patterns respectively. They are 83.2° and 70° for simulated E-and H-plane patterns at the same frequency. The comparison shows good agreement between the theoretical and simulated results that justify the veracity of the proposed method.

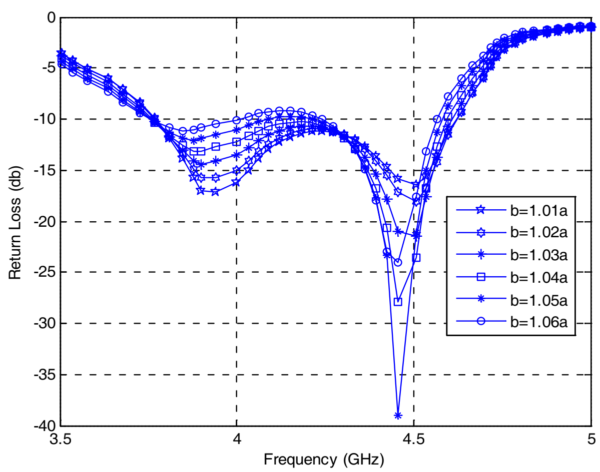

Figure 7: Return loss vs. frequency at different radius of parasitic disk (b) for $a = 13.233$ mm, $a_f = 7.94$ mm, $\varepsilon_{rd} = \varepsilon_{rp} = 2.45$, $\varepsilon_{ra} = 1.22$, $h_d = 1.522$ mm, $h_a = 4.764$ mm, and $h_p = 0.7609$ mm.

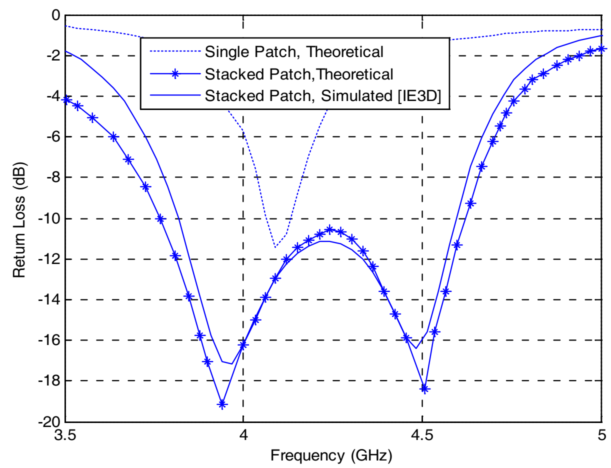

Figure 8: Optimum return loss curve for optimum design parameters: $a = 13.233$ mm, $b = 1.01a$, $a_f = 7.94$ mm, $\varepsilon_{rd} = \varepsilon_{rp} = 2.45$, $\varepsilon_{ra} = 1.22$, $h_d = 1.522$ mm, $h_a = 4.764$ mm, and $h_p = 0.7609$ mm.

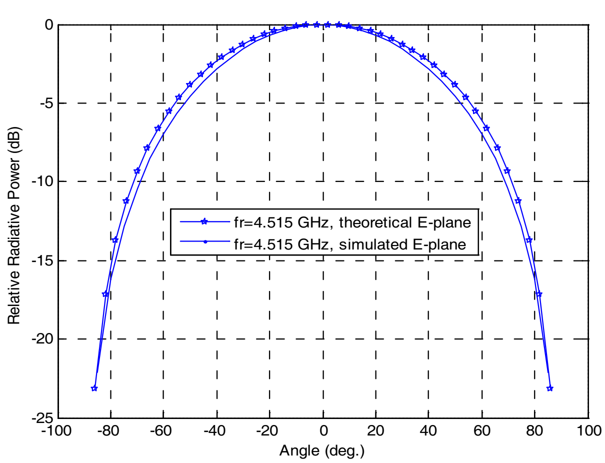

Figure 9: E-plane radiation patterns.

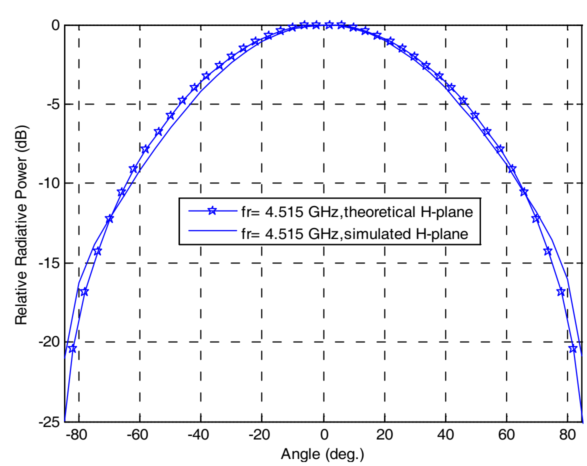

Figure 10: H-plane radiation patterns.

4. CONCLUSIONS

It may be concluded that due to dual resonance nature the antenna shows a broadband characteristics. Feed point location, radius of the parasitic disk, and air gap-spacing has profound effects on the antenna performance. It is also concluded that the bandwidth of the antenna may be broadened to as high as 19.79% with proper combination of interspacing of the patches. The radiation patterns are reasonably good for the use in both linear and planar arrays.

REFERENCES

1. Ansari, J. A., P. Singh, and N. P. Yadav, "Analysis of wideband multilayer patch antenna with two parasitic elements," *Microwave and Optical Technology Letters,* Vol. 51, 1397–1401, 2009.
2. Ansari, J. A., N. P. Yadav, and P. Singh, "Analysis of disk patch antenna with parasitic elements in single and multilayer structures," *Microwave and Optical Technology Letters*, Vol. 52, No. 4, 865–870, Apr. 2010.
3. Bhatnagar, P. S., J. P. Daniel, K. Mohdjoubi, and C. Terret, "Experimental study on stacked triangular microstrip antennas," *Electron. Lett.*, Vol. 22, 864–865, 1986.
4. IE3D Zeland software Inc., USA, version 14.05, 2008.
5. Zhong, S. S., G. Liu, and G. Qasim, "Closed form expressions for resonant frequency of rectangular patch antennas with multidielectric layers," *IEEE Trans. Antenna Propagat.* Vol. 42, 1360–1363, 1994.
6. Ribero, J. M., J. P. Damiano, and R. Staraj, "Accurate analysis and synthesis of annular microstrip antennas," *IEEE Proc. Microw. Antenna Propag.,* Vol. 144, 341–346, 1997.
7. Derneryd, A. G., "Analysis of the microstrip disc antenna element," *IEEE Trans. Antenna Propagat.,* Vol. 27, 660–664, 1979.
8. Garg, R., P. Bhartia, I. Bahl, and A. Ittipiboon, *Microstrip Antenna Design Handbook*, 339–354, Artech House, Norwood, MA, 2001.